Research Article

Journal of PeptideScience

Received: 17 June 2016 Revised: 7 October 2016 Accepted: 11 October 2016 Published online in Wiley Online Library

(wileyonlinelibrary.com) DOI 10.1002/psc.2934

Comparative analysis reveals amino acids critical for anticancer activity of peptide CIGB-552

Soledad Astrada,[a] Yolanda Gomez,[b] Exequiel Barrera,[c] Gonzalo Obal,[d,e] Otto Pritsch,[d] Sergio Pantano,[c] Maribel G. Vallespí[b] and Mariela Bollati-Fogolín[a]*

Because of resistance development by cancer cells against current anticancer drugs, there is a considerable interest in developing novel antitumor agents. We have previously demonstrated that CIGB-552, a novel cell-penetrating synthetic peptide, was effective in reducing tumor size and increasing lifespan in tumor-bearing mice. Studies of protein–peptide interactions have shown that COMMD1 protein is a major mediator of CIGB-552 antitumor activity. Furthermore, a typical serine-protease degradation pattern for CIGB-552 in BALB/c mice serum was identified, yielding peptides which differ from CIGB-552 in size and physical properties. In the present study, we show the results obtained from a comparative analysis between CIGB-552 and its main metabolites regarding physicochemical properties, cellular internalization, and their capability to elicit apoptosis in MCF-7 cells. None of the analyzed metabolites proved to be as effective as CIGB-552 in promoting apoptosis in MCF-7. Taking into account these results, it seemed important to examine their cell-penetrating capacity and interaction with COMMD1. We show that internalization, a lipid binding-dependent process, is impaired as well as metabolite–COMMD1 interaction, key component of the apoptotic mechanism. Altogether, our results suggest that features conferred by the amino acid sequence are decisive for CIGB-552 biological activity, turning it into the minimal functional unit. Copyright © 2016 European Peptide Society and John Wiley & Sons, Ltd.

Additional supporting information may be found in the online version of this article at the publisher's web site.

Keywords: cell penetrating peptide; COMMD1; amino acids; apoptosis

Introduction

Cationic antimicrobial peptides (AMPs), which are toxic to bacteria but not to normal mammalian cells, have been widely studied as an alternative therapy to chemotherapy in cancer treatment as they have proven to exhibit cytotoxic activity against cancer cells [1,3–5]. In chemoprevention, the use of antitumor peptides is of interest because, (i) these molecules are small, (ii) they show good cell diffusion and permeability, (iii) they affect one or more specific molecular pathways involved in carcinogenesis and (iv) they are usually not genotoxic [6]. The amphipathic structure and high net positive charge of AMPs are believed to play a major role in the ability to kill cancer cells but the molecular mechanisms underlying their anticancer activity are not clear [1,3–5].

Recently, a new synthetic peptide, L2, based on the cyclic amphipathic peptide $LALF_{32–51}$, derived from the Limulus sp, has been characterized as a potential antitumor agent [7]. Antitumor effects produced by L2 are based on its cell-penetrating capacity and its capability to elicit cytotoxicity in a variety of tumor cell lines and solid tumors established in mice [7]. In order to produce a more stable compound, modifications in the primary structure of L2 have been made resulting in a new generation of synthetic peptide: CIGB-552. Properties already described for L2, regarding its ability to reduce tumor volume and produce cytotoxic effect in tumor cell lines, are retained by CIGB-552 [8,9]. Moreover, we have shown that CIGB-552 stabilized COMMD1 levels, a protein involved in copper

* *Correspondence to: Mariela Bollati-Fogolín, Cell Biology Unit, Institut Pasteur de Montevideo, Mataojo 2020, 11400 Montevideo, Uruguay. E-mail: mbollati@pasteur.edu.uy*

a *Cell Biology Unit, Institut Pasteur de Montevideo, Mataojo 2020, 11400, Montevideo, Uruguay*

b *Pharmaceutical Department, Center for Genetic Engineering and Biotechnology, Havana, Cuba*

c *Biomolecular Simulations, Institut Pasteur Montevideo, Montevideo, Uruguay*

d *Protein Biophysics Unit, Institut Pasteur Montevideo, Montevideo, Uruguay*

e *Departamento de Inmunobiología, Facultad de Medicina, Universidad de la República, Avenida General Flores 2125, 11800, Montevideo, Uruguay*

Abbreviations: *AMPs, antimicrobial peptides; BSA, bovine serum albumin; CC_{50}, concentration of competitor required for inhibition of half the specific binding; CPPs, cell-penetrating peptides; DMSO, dimethyl sulfoxide; FBS, fetal bovine serum; FITC, fluorescein isothiocyanate; FSC, forward scatter; HPLC, high-performance liquid chromatography; IC_{50}, half maximal inhibitory concentration; ITC, isothermal titration calorimetry; MD, molecular dynamics; MFI, mean fluorescence intensity; PBS, phosphate-buffered saline; PFA, paraformaldehyde; POPC, 1-palmitoyl-2-oleoyl-sn-glycero-3-phosphocholine; POPG, 1-palmitoyl-2-oleoyl-sn-glycero-3-phospho-(1′-rac-glycerol); SSC, side scatter; SD, standard deviation; SRB, sulforhodamine B; TCA, trichloroacetic acid; TFA, trifluoroacetic acid; TMB, tetramethylbenzidine; US, untreated unstained cells.*

homeostasis, sodium transport, and the NF-κB signaling pathway [2,8,10]. COMMD1 expression is needed to produce pro-apoptotic effects on NCI-H460 lung carcinoma-derived cell line [8]. When exposed to BALB/c mice serum, CIGB-552 shows a typical serine-protease degradation pattern from which several metabolites are derived [9]. Three of these metabolites are metabolite 5, 1a, and 3 whose first characterization showed a decrease in their cell-penetrating capacity in NCI-H460 and HT-29 cell lines when compared to CIGB-552 [9]. Furthermore, the IC_{50} (half maximal inhibitory concentration) values obtained for these metabolites in both cell lines were higher than those observed for CIGB-552 [9]. The chemical optimization strategy of a therapeutic peptide is based on structure–activity relationship studies of newly synthesized peptide derivatives with the aim of improving bioavailability, reducing elimination and biodegradation, and increasing selectivity or affinity to its receptor or target [11]. In this study, we compare the physicochemical properties, pro-apoptotic effects, COMMD1 and lipid binding capacities of CIGB-552 and its main derived metabolites. Our studies show for the first time that CIGB-552 and metabolite 5 have similar behavior regarding lipid-binding affinity and structural conformation. However, because of affinity for COMMD1, CIGB-552 represents the minimum active sequence capable of elicit pro-apoptotic effects in a tumor-derived cell line.

Materials and Methods

Reagents and Chemicals

Unless otherwise indicated, all chemicals used were of the highest grade available and purchased from Sigma-Aldrich. Culture media, fetal bovine serum (FBS), and consumables for cell culture were obtained from Life Technologies (USA), GE Healthcare, and Greiner. All reagents for peptide synthesis were of synthesis grade. Reagents for chromatography were of high-performance liquid chromatography (HPLC) grade. Trifluoroacetic acid (TFA) was from Panreac (USA), acetonitrile was from Caledon (Canada), and water was of ultrapure quality. The NH_4HCO_3 was from Merck (Germany).

Peptide Synthesis

Peptide CIGB-552 and its analogous metabolites were synthesized on a solid phase and purified by reverse-phase-HPLC to >95% purity on an acetonitrile/H_2O trifuoracetic acid gradient and confirmed by ion-spray mass spectrometry (Micromass, Manchester, UK) [9]. Lyophilized peptides were reconstituted in apyrogenic water for *in vitro* experiments. The analogous metabolite peptides used in this work contain deletions of consecutive amino acids at the N and C-termini of the CIGB-552 peptide (Table 1). The carboxy-fluorescein fluorophore was attached selectively by an amide bond to the N-terminus of the peptide sequences during the synthesis of the peptide in solid phase performed using the Fmoc/t-Bu chemistry. The linking is direct to the N-terminus of the peptide; there are no additional residues.

Cell Line and Culture Medium

MCF-7 (ATCC, HTB-22) cells were cultured in DMEM supplemented with Glutamax and 10% (v/v) FBS. Cells were routinely propagated in 25 or 75 cm^2 tissue culture flasks at 37 °C, 5% CO_2 in a humidified incubator until reaching approximately 70% confluence. Cells were subsequently trypsinized, concentration was adjusted, and used for different experimental settings. Cells were cultured for no longer than 10–15 passages.

Sulforhodamine B Assay

Antiproliferative assays were essentially performed as previously described [12,13]. Cells were seeded in 96 well cell culture plates (GLS3595, Costar, EUA) and maintained in culture for 24 h prior to adding CIGB-552 and its derived metabolites. Peptides were added in concentrations ranging from 3000 to 6 μM to the cells (1×10^4cells/well) and incubated for 48 h in serum-containing medium at 37 °C in 5% CO_2. Subsequently, 50 μl of 80% (v/v) trichloroacetic acid (TCA) solution was added, and cells were incubated for 1 h at 4 °C. Finally, 100 μl of the Sulforhodamine B (SRB) solution was added to the wells, and absorbance was measured at 492 nm. Each sample point was done in triplicates, and experiments were carried out twice. IC_{50} values were obtained from the respective dose–response curves (Supplementary Fig. S2).

Apoptosis Assays: Annexin V and Caspase 7

MCF-7 cells were seeded in 12 well plates (1×10^5 cell/well) and cultured for 24 h. Peptides CIGB-552, 5, 1a and 3 were added to a final concentration of 300 μM (250 μl/well, 4.23×10^{-13} mol/cell) in serum-free medium, and cells were incubated at 37 °C for 24 h. In order to compare the pro-apoptotic capacity of CIGB-552 derived metabolites with the CIGB-552 itself, peptide concentration was selected according to previously optimized results in the MCF-7 cell line (Supplementary Fig. S1). Finally, supernatants and cells were collected and resuspended either in Annexin V buffer 25 mM HEPES, 140 mM NaCl, 1 mM EDTA, pH 7.4, 0.1% (v/v) bovine serum albumin (BSA) or medium for Caspase 7 assay. FITC-conjugated Annexin V (Life Technologies, USA) or CellEvent™ Green (Life Technologies, USA) was added to the cells (for Annexin V or Caspase 7 assays, respectively) and incubated for 15–30 min. Samples were acquired in a Cyan ADP Analyzer (Beckman Coulter, USA) equipped with 488-nm laser. Fluorescence emissions were detected using band-pass filters 530/40. For each sample, 10 000 counts gated on a forward scatter (FSC) *versus* side scatter (SSC) dot plot, excluding doublets

Table 1. Main physicochemical properties observed for CIGB-552 and its derived metabolites

ID	Sequence	Molecular weight	Hydrophobicity	Hydrophilicity	Net charge	Isoelectric point
CIGB-552	HARIKPTFRRLKWKYKGKFW	2647.51	−0.39	0.25	+8.5	7.65
5	IKPTFRRLKWKYKGKFW	2283.06	−0.35	0.17	7	7.56
1a	IKPTFRRLKWKYKG	1821.45	−0.41	0.41	6	7.68
3	IKPTFRRLKW	1344.81	−0.37	0.21	4	7.67

were recorded. Summit v4.3 software was used for data acquisition and analysis. Fold change was calculated as the ratio between Annexin V (% of positive cells) or Caspase 7 (% of positive cells) and control (% of positive cells).

Competitive ELISA

Polystyrene plates (Costar, USA) were coated with recombinant protein COMMD1 (10 μg/ml) in coating buffer ($NaCO_3$/$NaHCO_3$ pH = 9.6). Plates were incubated overnight at 4 °C and washed three times with phosphate-buffered saline (PBS) 1X 0.1% Tween-20 (washing solution). Plates were blocked with milk 1% (w/v) in PBS 1X 2 h at 37 °C and then washed 4 times with washing solution. Binding of metabolites to the immobilized recombinant COMMD1 was evaluated by competition with biotinylated-CIGB-552 at 0.021 μM. Concentration curves for metabolites were prepared by making serial dilutions (1:2) in a range from 10 to 0.005 μM and added to the ELISA plates coated with recombinant COMMD1 together with the biotinylated CIGB-552 at a fixed concentration. Plates were incubated 1 h at 37 °C and washed 5 times with washing solution. Anti-Biotin-Peroxidase antibody (Sigma A4541), at a 1:5000 dilution, was used to detect biotinylated CIGB-552 bound to COMMD1. Plates were washed 6 times with washing solution and the substrate solution consisting of 3,3,5,5′ tetramethylbenzidine (TMB), dimethyl sulfoxide (DMSO) in a NaAc 0.1 M pH = 5.2 solution with 0.2% (v/v) of hydrogen peroxide was added. Development of the reaction was performed in the dark and stopped by adding sulphuric acid 0.5 M. Absorbance was measured at 450 nm in a microplate reader (SUMA). COMMD1 binding capacity was calculated using the following formula: $1 - ([OD]_{sample} - [OD]_{min})/([OD]_{max} - [OD]_{min})$; $[OD]_{sample}$, optical density in the presence of metabolites peptide; $[OD]_{min}$, background of the assay; $[OD]_{max}$, optical density in the presence of CIGB-552-biotynilated at 0.021 μM.

Internalization Assay – Flow Cytometry and Confocal Microscopy

MCF-7 cells were seeded in 12-well plates (1×10^5 cells/well) and cultured in D-MEM supplemented with Glutamax, 10% (v/v) FBS, at 37 °C for 24 h. For those samples where internalization was analyzed by microscopy, round coverslips were placed into the wells prior to cell seeding. Subsequently, FITC-conjugated peptides, CIGB-552, 5, 1a, and 3 were added to the cells to a final concentration of 50 μM (250 μl/well, 7.04×10^{-14} mol/cell) and were incubated for 1 h at either 4 °C or 37 °C. This concentration was previously optimized and selected in order to obtain consistent results and/or to avoid possible artifacts (Supplementary Fig. S3). Moreover, concentrations used for internalization and apoptosis assays proved not to be conditions under which CIGB-552 or its derived metabolites may show oligomerization (Supplementary Fig. S4). For flow cytometry readout, culture medium was removed, cells were washed using PBS and surface-bound FITC-peptide was quenched with 0.4% (w/v) Trypan Blue solution; cells were trypsinized and resuspended in medium. Samples were acquired in a Cyan ADP Analyzer (Beckman Coulter, USA) equipped with 488-nm laser. Fluorescence emissions were detected using band-pass filters 530/40. For each sample, 10 000 counts gated on an FSC *versus* SSC dot plot, excluding doublets were recorded. Summit v4.3 software was used for data acquisition and analysis. Fold change was calculated as the ratio between mean fluorescence intensity (MFI) values of treated samples and control samples. For microscopy assays, cells were fixed in 4% (w/v) paraformaldehyde (PFA) for 15 min, permeabilized using 0.2% (v/v) Tween 20 solution in PBS and nuclei were stained using TOPRO-3 (1 μM, Life Technologies) and CellMask™, membrane marker (1:2000, Life Technologies). All images were taken using laser spectral confocal microscope Leica TCS SP5 equipped with a 63× NA 1.42 oil immersion objective and 488-nm, 543-nm, and 633-nm laser lines were used. Emission for each channel was collected sequentially to avoid bleed-through between signals. In order to define internalization patterns optical sections were scanned at intervals of 0.3 μm. Quantification of the number of fully loaded cells was performed using 10 single optical sections for each metabolite and the CIGB-552 peptide. Image processing and counting were done using Icy 1.7.3.1v imaging software [14].

Rab5A and Anti-Fibrillarin Immunodetection

MCF-7 cells were seeded in 12-well plates containing round coverslips (1×10^5 cells/well) and cultured in D-MEM supplemented with Glutamax, 10% (v/v) FBS, at 37 °C for 24 h. For early endosome staining, CellLight® Early Endosomes-RFP BacMam 2.0 (Life Technologies) was used at a concentration of 10 particles per cell and incubated with the cells overnight. Subsequently, FITC-conjugated peptides were added to a final concentration of 50 μM (250 μl/well, 7.04×10^{-14} mol/cell), and cells were incubated at 37 °C for 1 h. Cells were fixed in 4% (w/v) PFA for 15 min, permeabilized using 0.2% (v/v) Tween 20 solution in PBS and nuclei were stained with TOPRO-3. For fibrillarin staining, fixed cells were permeabilized and blocked with 2% (w/v) bovine serum albumin in PBS (BSA-PBS) for 1 h. Primary antibody, mouse monoclonal anti-Fibrillarin (1:1000, AFB01, Labome) was diluted in BSA-PBS, added and incubated overnight at 4 °C. Three washing steps were performed using 0.2% (v/v) Tween 20 solution in PBS solution. Goat anti-Mouse IgG (H + L) secondary antibody, Cy3 conjugated (Life Technologies) diluted 1:1000 in BSA-PBS was added and incubated for 1:30 h. Finally, nuclei were stained with TOPRO-3. All images were taken using laser confocal microscope Leica TCS SP5 equipped with a 63× NA 1.42 oil immersion objective and 488-nm, 543-nm, and 633-nm laser lines were used. Emission for each channel was collected sequentially to avoid bleed-through between signals. Optical sections scanned at intervals of 0.3 μm were taken, and image processing was done using Icy 1.7.3.0v imaging software [14].

Preparation of Liposomes

A 0.5 mM solution POPC:POPG (80:20 molar ratio) dissolved in methanol–chloroform (1:1 v/v) was prepared in a round bottom glass flask. The solvent was evaporated using a N_2 atmosphere. Multilamellar vesicles were prepared by hydration of dried lipids in hot buffer (50 °C) (10 mM HEPES, 150 mM NaCl, and 1 mM EDTA pH 7.4) with vigorous mixing using vortex. The suspension was incubated during 1 h at 50 °C and 1000 rpm in a Thermomixer (Eppendorf). Unilamellar liposomes were produced by Mini-Extruder Extrusion Technique (Avanti Polar Lipids, Inc.) using first 1 μm and then 200-nm membrane filters (Whatman®Nuclepore Track-Etched Membranes). The suspension was passed through each membrane filter 11 times.

Isothermal Titration Calorimetry

Isothermal titration calorimetry (ITC) was performed using a VP-ITC microcalorimeter (Malvern). For all experiments, liposomes were loaded into the sample cell and titrated with peptide solution loaded into the syringe, maintaining the equipment at 37 °C. For each experiment set and before loading the microcalorimeter, peptide and liposome solutions were thoroughly degassed for 10 min under constant stirring using a Thermovac (Microcal). To optimize experimental conditions, preliminary experiments were carried out. Both liposome concentration inside the sample cell and peptide concentration in syringe were maintained at 0.5 mM. Injection schedule consisted of a first pre-injection of 1 μl first, followed by subsequent 10-μl injections spaced by 5 min until reach saturation (25–30 injections), under a stirring regime of 390 rpm. Data was analyzed using Origin 7.0 software provided by the manufacturer, performing baseline and blank corrections, and subsequent molar heat integration.

Molecular Dynamics Simulations

Molecular dynamics (MD) simulations were performed using the SIRAH force field [15]. Computational details are provided in the Supporting Information. Briefly, simulations of the CIGB-552 peptide and its derived metabolites 5, 1 and 3a were performed in aqueous solution and in the presence of a phospholipid's bilayer using a random conformation for each peptide. All simulations were performed at the coarse-grained level, and nearly atomistic detail was recovered using SIRAH tools [16].

Statistical Analysis

Data was expressed as the mean ± SD of triplicates of one representative experiment; three independent experiments were executed. Statistic calculations were performed using Statistica software, STATSOFT, Hamburg, Germany. Differences were considered statistically significant when $P < 0.05$ using Mann–Whitney U test.

Results

CIGB-552 and Derived Metabolite Physicochemical Properties

Previous results obtained for three CIGB-552 degradation derived metabolites (referred to as 5, 1a and 3) indicated that differences in their sequence may affect their functionality [9]. However, theoretical prediction of their cell penetrating capacity estimated by two different servers CPPpred and C2pred [17,18] showed no differences on the probability of CIGB-552 and its derived metabolites to be considered as cell-penetrating peptides (CPPs) (Supplementary Table 1). Furthermore, using theoretical predictions of the amino acids physicochemical properties (PEPstrMOD, http://osddlinux.osdd.net/raghava/pepstrmod) such as molecular weight, hydrophobicity, hydrophilicity, net charge, and isoelectric point were determined [19]. CIGB-552 derived metabolites showed no great differences regarding hydrophobicity, hydrophilicity, and isoelectric point. However, a reduction in the net charge was observed, a key feature involved in lipid membrane–AMP interaction [1,3–5,20,21]. This reduction reached up to a 50% in the smallest peptide, metabolite 3. Obtained values are summarized in Table 1.

CIGB-552 Induces Apoptosis but its Derived Metabolites do not

Previous results obtained for the MCF-7 cell line showed that the CIGB-552 was capable to elicit a pro-apoptotic effect (Supplementary Fig. S1) as well as it has been reported for several other cell lines [7,8]. However, cytotoxic effect and pro-apoptotic capacity of CIGB-552 derived metabolites have not yet been characterized in the MCF-7 cell line. Therefore, we decided to explore the cytotoxic effects of the derived metabolites by using SRB assay, a protein staining assay for the *in vitro* measurement of protein content that has been widely used as a method for cytotoxicity screening [12,13]. Peptides were added to the MCF-7 cells in a range of concentrations form 3000 to 6 μM and incubated for 48 h. Inhibition dose–response curves obtained from these assays showed a reduced capacity of the metabolites to inhibit cell proliferation (Table 2 and Supplementary Fig. S2). We further explored whether its derived metabolites were able to elicit an apoptotic effect despite the observed differences in IC_{50} values obtained. In order to accomplish that we selected two of the most common methods for apoptosis detection: Annexin V staining and caspase activation [22]. Based on the fact that Caspase 3 is absent in the MCF-7 cell line because of a functional deletion of CASP-3 gene [23,24], Caspase 7 activation was evaluated. No significant differences were observed between metabolite treatments and control cells neither in Caspase 7 activation assay nor in Annexin V staining, showing that under these conditions metabolites were unable to elicit a pro-apoptotic effect on the MCF-7 cell line (Figure 1A). However, CIGB-552 confirmed its capacity to induce apoptosis (Figure 1A) as it has been previously reported for other tumor cell lines [7,8]. In both assays, CIGB-552 treatment resulted in a two-fold increase in the apoptotic process when compared to control and metabolites-treated cells (Figure 1B).

Derived Metabolites Showed Reduced Binding Capacity to COMMD1 *In Vitro*

COMMD1 has been characterized by both yeast two hybrid and pull down assays as one of the main targets of CIGB-552 peptide action [8]. Moreover, lack of COMMD1 expression results in the absence of apoptosis induced by CIGB-552 treatment [8]. To date, no data regarding CIGB-552 derived metabolite capability to interact with the target protein COMMD1 has been produced. Therefore, we evaluated the ability of metabolites to bind COMMD1 through a competitive ELISA assay. In this experiment, a constant amount of biotinylated CIGB-552 (0.021 μM) was mixed with metabolites in a range of concentration from 10 to 0.005 μM and then added to the pre-coated wells with recombinant COMMD1. The biotinylated CIGB-552 bound to COMMD1 was detected by incubating with anti-biotin-peroxidase monoclonal

Table 2. Cytotoxicity of CIGB-552 and its derived metabolites was evaluated by SRB assay. IC_{50} (μM) values were obtained showing an increase in the IC_{50} of the smaller metabolites

ID	Sequence	IC50 (μM)
CIGB-552	HARIKPTFRRLKWKYKGKFW	379.1 ± 8.6
5	IKPTFRRLKWKYKGKFW	493.4 ± 12.9
1a	IKPTFRRLKWKYKG	1540.8 ± 17.5
3	IKPTFRRLKW	2431.0 ± 1.6

Journal of PeptideScience

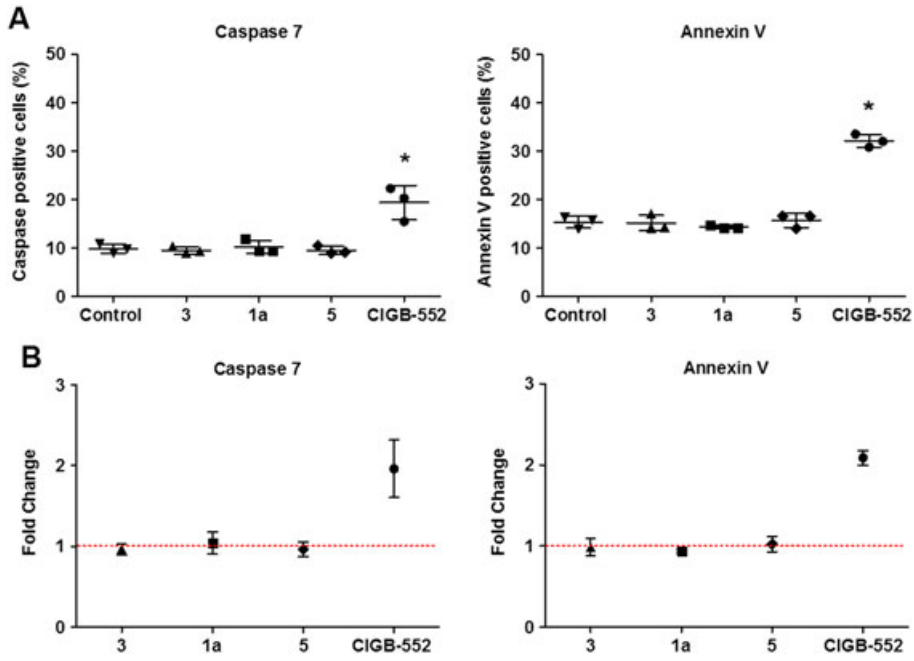

Figure 1. Apoptosis assessment using Caspase 7 activity assay and Annexin V staining. A, CIGB-552 produces an increase in both Caspase 7 activity and Annexin V staining when compared to its derived metabolites (* $p < 0.05$ Mann–Whitney *U* test). B, Apoptosis levels detected in CIGB-552 treated cells were at least twofold higher than those observed for control and metabolite-treated cells. Fold change was calculated as the ratio between Caspase 7 (% of positive cells) or Annexin V (% of positive cells) and control (% of positive cells).

antibody. Results represent the displacement of biotinylated CIGB-552-COMMD1 binding produced by a specific concentration of peptide. Both, CIGB-552 and metabolite 5, competed with the biotinylated CIGB-552 to bind COMMD1. On the other hand, no competition was observed for 1a and 3 indicating a diminished affinity of these metabolites for COMMD1 (Figure 2). Concentrations of competitor required for inhibition of half the specific binding (CC_{50}) were also calculated (Table 3).

Cell Penetrating Capacity and Mechanisms Involved in CIGB-552 and its Derived Metabolite Internalization

In order to exert its apoptotic effects through COMMD1, internalization of CIGB-552 by cells is required; this has been described

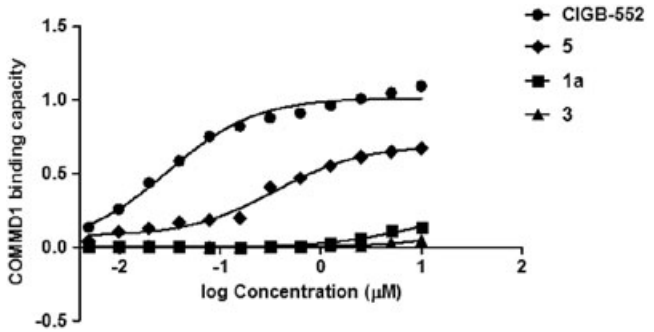

Figure 2. The *in vitro* capacity of derived metabolites to bind COMMD1 was evaluated by a competitive ELISA assay. Metabolites and biotinylated CIGB-552 were added to the COMMD1-coated ELISA plates. The graphic represents the capacity of metabolites to displace the CIGB-552-COMMD1 binding; a representative curve from three independent experiments is shown. Not only CIGB-552 showed displacement capacity but also metabolite 5 proved to be able to displace COMMD1-CIGB-552 binding. Metabolite 1a and metabolite 3 were not able to produce any effect in such conditions.

as a key feature that makes this novel synthetic peptide an interesting candidate for therapy. In such case, CIGB-552 can be considered as a CPPs [21]; therefore, different internalization mechanisms could be proposed. CPPs have been described to enter cells either by the classical endocytic pathway or through an energy-independent mechanism referred to as transduction. Besides the requirements needed for each mechanism, different internalization patterns are also observed inside the cells. Endocytosis produces a punctuated pattern consequence of peptide internalization into endocytic vesicles. Meanwhile, transduction by direct membrane penetration results in fully loaded cells displaying an homogeneous distribution throughout the cytoplasm and nucleoplasm [25,26]. Therefore, as a first approach, confocal microscopy using FITC-conjugated peptides was performed, and the internalization patterns were studied. Both punctuated and fully loaded patterns were identified for CIGB-552 and its derived metabolites (Figure 3A). The frequency of fully loaded cells, estimated as the percentage of the total number of cells counted was also evaluated. CIGB-552 showed a significant increase in fully loaded cells compared to its derived metabolites (Figure 3B). Moreover, expression of two different proteins Rab5A and Fibrillarin was analyzed. Rab5A is a small GTPase which has been found to be expressed in early endosomes [27], and Fibrillarin, which possesses methyltransferase activity, is a commonly used marker of active nucleoli [28]. Therefore, by using these two proteins, we were allowed to define CIGB-552 localization with respect to both endosomes and nucleoli. Co-localization was found among CIGB-552 and these two markers (Figure 4), indicating that this peptide is effectively able to enter cells through different mechanisms. Moreover, co-localization was found between CIGB-552 derived metabolites and Rab5A (Supplementary Figure S5). In order to quantify the cell-penetrating capacity of CIGB-552 and its derived metabolites, flow cytometry assays were performed

Table 3. COMMD1 affinity was measured by competitive ELISA. CC_{50} (μM) the concentration of the competitor required to compete for half the specific binding. R^2: square regression coefficient. ND: not determined

ID	Sequence	CC_{50} (μM)	R^2
CIGB-552	HARIKPTFRRLKWKYKGKFW	0.4 ± 0.046	0.99
5	IKPTFRRLKWKYKGKFW	1.4 ± 0.26	0.98
1a	IKPTFRRLKWKYKG	ND	ND
3	IKPTFRRLKW	ND	ND

by incubating MCF-7 cells with FITC-conjugated peptides. Fluorescence intensity histogram overlays showed a shift towards higher fluorescence intensity values for both CIGB-552 and metabolite 5 (Figure 5A). MFI values corresponding to metabolites 1a and 3 showed significant differences between both CIGB-552 and metabolite 5 (Figure 5B). CIGB-552 confirmed its high penetrating capacity by displaying the highest MFI values. These results suggest that both CIGB-552 and its derived metabolites may use different internalization mechanism and that CIGB-552 has the highest cell penetrating capacity.

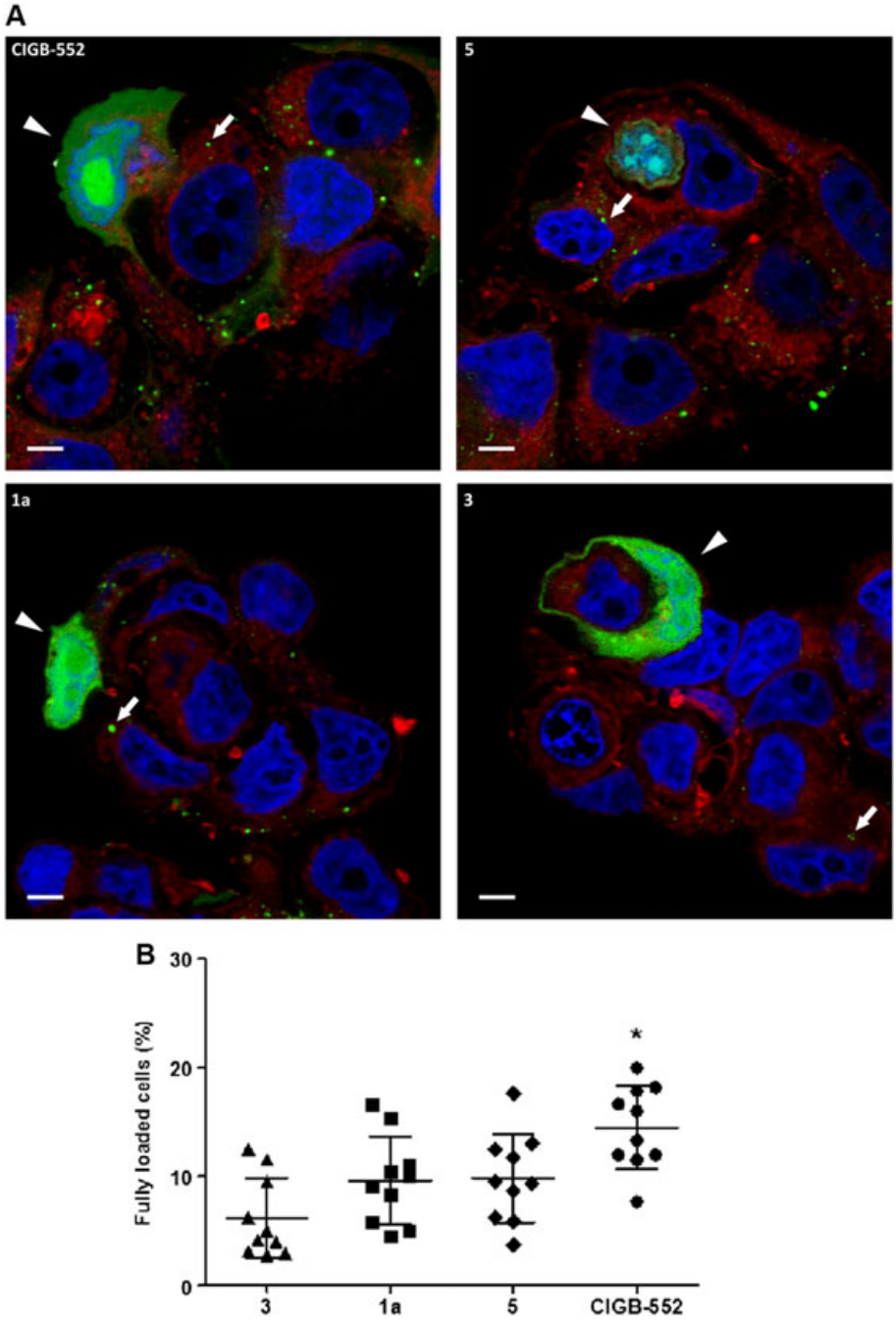

Figure 3. A, Confocal micrographs showing different internalization patterns. Fully loaded cells (arrow heads) and punctuated pattern cells (arrows), each of them corresponding to both transduction and endocytic mechanisms, are observed for CIGB-552 and its derived peptides (scale bar = 5 μm). B, Percentage of fully loaded cells found in CIGB-552 and its derived metabolites, a significant increase was observed between CIGB-552 and its derived metabolites ($p < 0.005$ Mann–Whitney *U* test). Total number of counted cells: CIGB-552 $n = 237$, metabolite 5 $n = 233$, metabolite 1a $n = 197$ and metabolite 3 $n = 274$.

Journal of PeptideScience

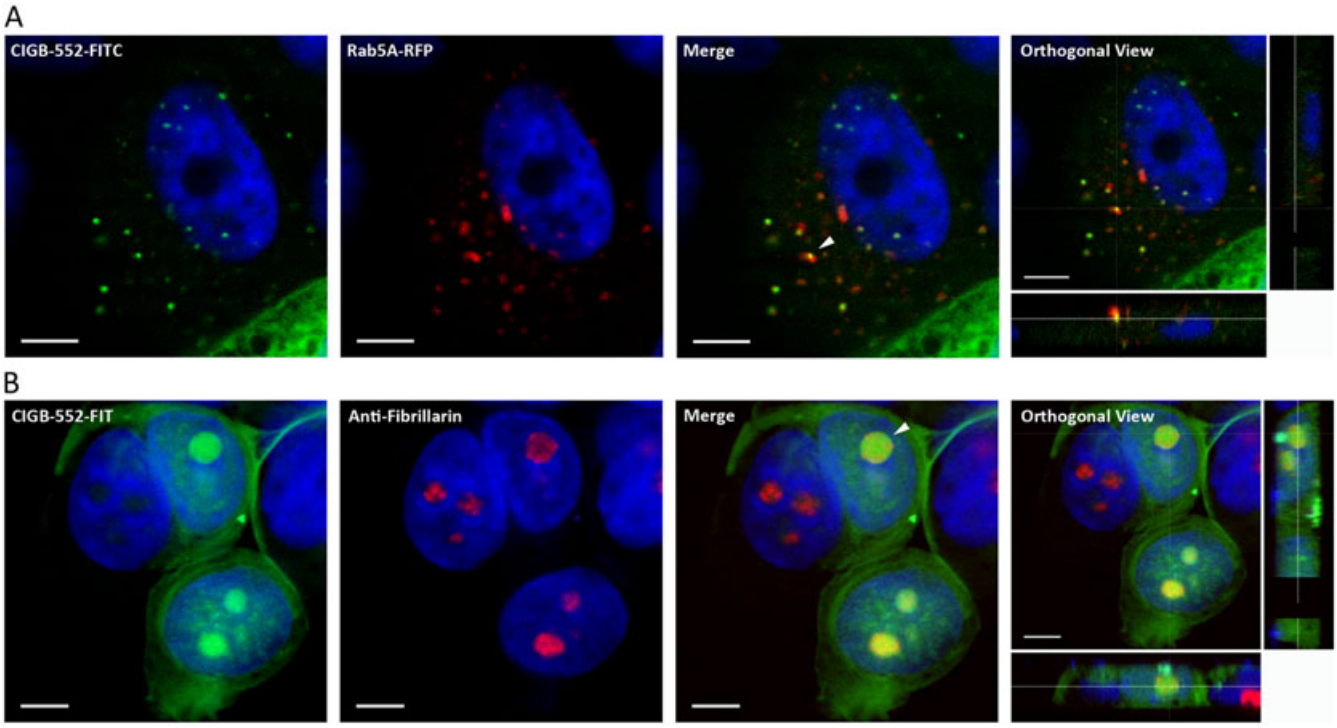

Figure 4. Confocal micrographs of Rab5A and Fibrillarin staining. A, Rab5A protein, an early-endosome marker (red) showed co-localization spots with CIGB-552-FITC conjugated peptide in the cytoplasm (arrow heads). B, Fibrillarin, a ribonucleo-protein located at the nucleolus (red), showed co-localization with CIGB-552-FITC conjugated peptide (scale bar = 5 μm).

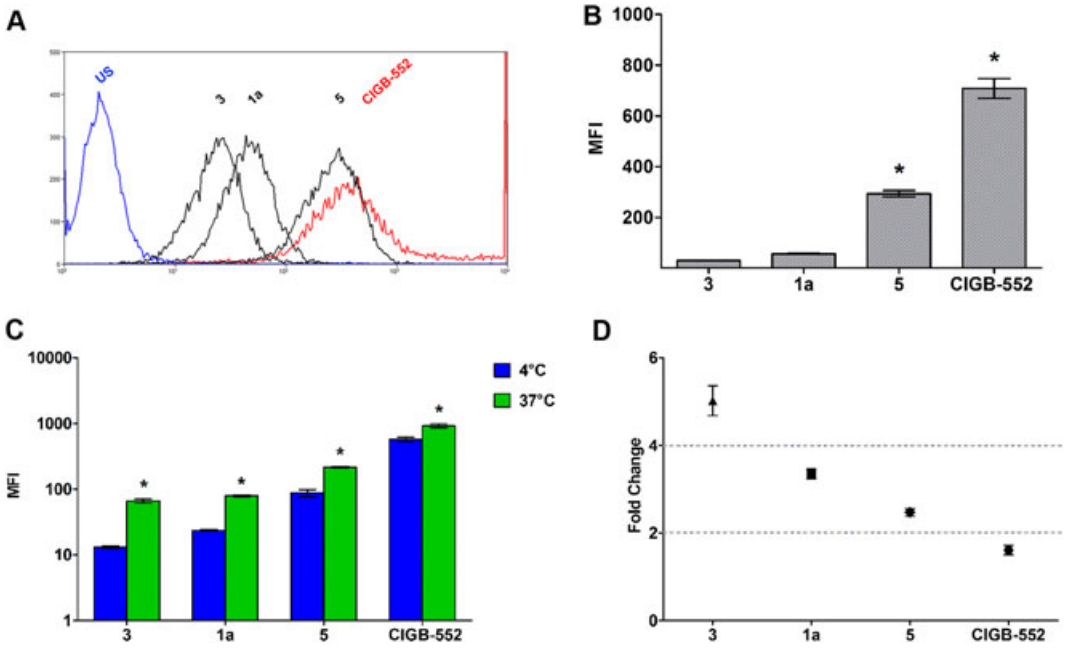

Figure 5. Cell-penetrating capacity of CIGB-552 and its metabolites was assayed using FITC-labeled peptides and evaluated by flow cytometry. Results obtained from one representative assay are shown. A, FITC fluorescence intensity histogram overlays show a shift towards high fluorescence intensity values for CIGB-552 and metabolite 5 when compared to metabolites 1a and 3 (US: untreated unstained cells). B, MFI values obtained from histograms displayed in A confirm the higher internalization levels for both CIGB-552 and 5 than those observed for 1a and 3 (* $p < 0.05$ Mann–Whitney *U* test). C, cell penetrating capacity was also evaluated at 37° and 4 °C, MFI values obtained at 37 °C were higher when compared to those obtained at 4 °C (* $p < 0.01$ Mann–Whitney *U* test). D, Fold change obtained from the ratio of MFI 37 °C/MFI 4 °C, highest fold change were observed for metabolite 1a and metabolite 3 indicating a stronger effect of energy-dependent internalization mechanism in the two smallest metabolites.

Differential Effect of Temperature on Cell Penetrating Capacity May Indicate Differential Internalization Mechanisms for CIGB-552 and its Derived Metabolites

As described previously, two alternative mechanisms are reported which vary in energy dependence and temperature required. While endocytosis is an energy-dependent process which occurs mainly at 37 °C, transduction is not, and may occur at lower temperatures (4 °C), also both mechanisms could be present at the same time [25,26]. A commonly used approach to determine which one of these processes is present is to perform internalization assays at different temperatures. We followed the same strategy described previously using FITC-conjugated peptides in MCF-7 cells which were incubated for 1 h at either 4 °C or 37 °C and subsequently analyzed by flow cytometry. At 37 °C, given the MFI values obtained, all peptides showed an increase in their internalization compared with the 4 °C condition (Figure 5C). However, the effect of temperature in the internalization process may appear to be stronger for those metabolites with shorter amino acid sequences as represented by the fold change 37°/4 °C (Figure 5D). Fold change was calculated as the ratio between the MFI values obtained at 37 °C and values obtained at 4 °C. Therefore, considering the internalization patterns observed and the impact of temperature, these results may indicate that transduction has a greater contribution to internalization mechanisms in CIGB-552 than in its derived metabolites.

Lipid Binding Capacity is Reduced in CIGB-552 Metabolites

Peptide–lipid interaction is a key feature for peptide internalization and is based on peptide structure. Having proved that CIGB-552 derived metabolites differ from CIGB-552 in their cell-penetrating capability, we decided to evaluate their ability to interact with lipid membranes. In order to mimic a cell membrane structure, we used synthetic liposomes as a model, consisting of a mixture of polar and non-polar lipids like POPC:POPG (80:20). Analysis of peptide–liposome interaction was performed by ITC, which implies the direct measurement of the heat generated or absorbed when molecules interact [29]. Given the lack of information about the underlying mechanism of liposome–peptide interaction, which consequently hampers model-specific fitting, we used the enthalpic titration data for evaluating the presence or absence of binding in a qualitative manner. In this sense, under the tested conditions, the heats of reaction observed for CIGB-552 as well as for metabolite 5 are in agreement with those expected for a binding process [29]. However, the heats of reaction observed for the two smallest metabolites (1a and 3) were almost constant throughout the assay, as expected for a dilution process, indicating that in such conditions, no binding was occurring [29] (Figure 6).

MD Simulations of CIGB-552 and its Derived Metabolites

Aimed to gain a structural insight into the peptide–membrane interactions, we performed MD simulations in aqueous solution and in the presence of a lipid bilayer. In water, all peptides sample a wide range of unstructured conformations, and only metabolite 1a showed a flickering tendency to sample beta-stranded conformations in different amino acids. Despite this, none of the peptides show a clear tendency to adopt stable and long-lasting secondary structures (see Figure 7A for representative structures). However, the two longest peptides present a conserved structural motif in which the two tryptophans and the tyrosine form a hydrophobic cluster that brings together the C-terminal carboxylate moieties and one arginine residue, forming a stable salt bridge interaction leading to a looped conformation (Figure 7B). Indeed, tryptophan–tryptophan and arginine–C-terminal carboxylate distances in both systems display very stable interactions (Figure 7C). Simulations in the presence of a phospholipid membrane indicate that, within the simulated timescale, nearly 10% of the peptides get inserted into the membrane regardless their extension. Membrane incorporation proceeds by first inserting the N-terminal, followed by partially solvated basic amino acids (Figure 7A), while C-terminal carboxylates in metabolites 1a and 3 remain exposed to the solvent. This agrees with previously described mechanisms for basic peptide penetration [30], and is putatively caused by a higher energetic cost to dehydrate C-terminal moieties [31]. In contrast, CIGB-552 and metabolite 5 maintain the looped conformation in the membrane environment. Although tryptophan–tryptophan interactions become looser within the hydrophobic media, the salt bridge remains very stable (Figure 7D), putatively contributing to the insertion of the C-terminal. Considering that simulations are completely unrelated, the structural resemblance of CIGB-552

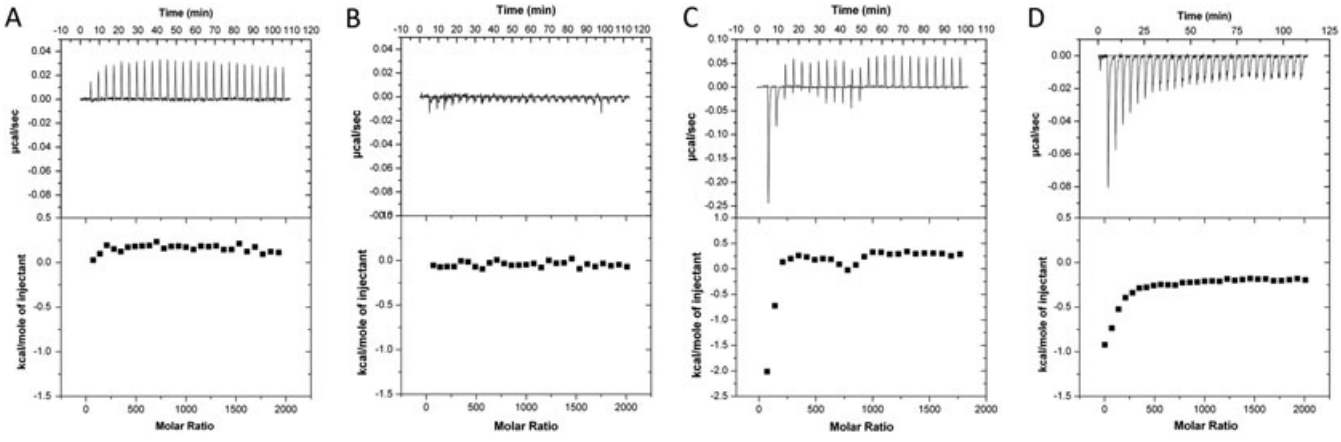

Figure 6. Isothermal titration calorimetry. A, metabolite 3. B, metabolite 1a. C, metabolite 5. D, CIGB-552. The upper panel represents the heat release (raw data) during each injection and in the lower panel raw data was integrated to yield the experimental heats of reaction. Binding-like curves are observed for CIGB-552 and metabolite 5, while metabolites 1a and 3 curves are almost constant throughout the assay probably corresponding to a dilution process pattern.

Journal of PeptideScience

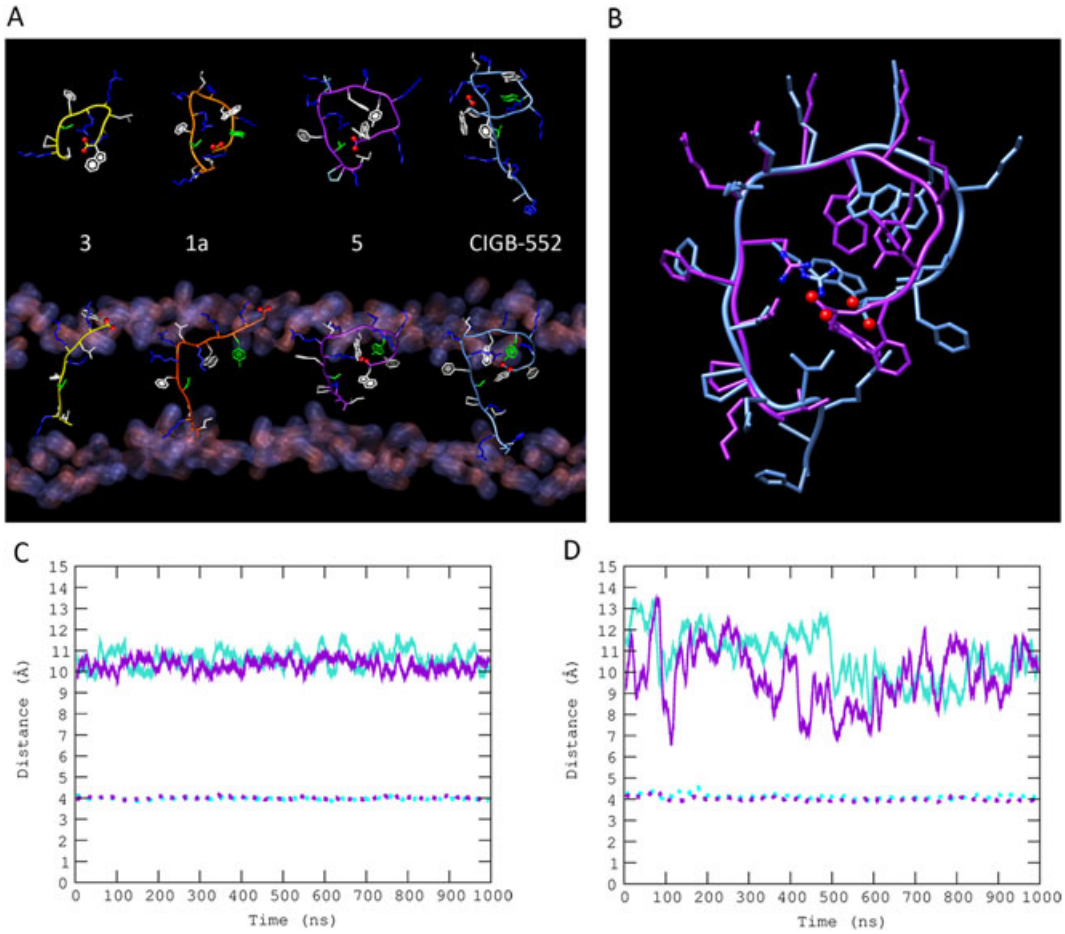

Figure 7. A, Different conformations adopted by CIGB-552 and its derived metabolites both in bulk solvent (upper panel) and inserted into the lipid bilayer (lower panel). CIGB-552, 5, 1a, and 3 backbones are colored in light blue, purple, orange and yellow, respectively. B, Superimposed structures of CIGB-522 (light blue) and metabolite 5 (purple) in their transmembrane conformations. Salt bridges between arginine side chain and COO^- are emphasized showing N and O atoms with blue and red spheres, respectively. C, Distances between tryptophans residues (solid lines) and Arg-COO^- terminal (dotted lines) for compounds CIGB-522 (light blue) and metabolite 5 (purple) as a function of time in solution. D, Distances between tryptophans residues (solid lines) and Arg-COO^- terminal (dotted lines) for compounds CIGB-522 (light blue) and metabolite 5 (purple) as a function of time within the lipid bilayer.

and metabolite 5 within the membrane environment is notable (Figure 7B), suggesting a conserved mode of interaction not present in the two shorter peptides.

Discussion

Discovering new therapeutic alternatives to cancer treatment has been one of the major forces driving cancer research in the last years, fueled by cytotoxic side effects and resistance development observed in the traditional available methods. Anti-microbial peptides have arisen as interesting candidates because their amphipathic structure allows them to interact directly with negatively charged cell membranes, a common feature that distinguishes malignant from non-malignant cells [1,3–5]. These small peptides are capable of efficiently affecting several cellular pathways without accumulation of toxic derivatives [6]. In developing a peptide anticancer agent manipulation of the amino acid sequence, net charge, secondary structure, oligomerization ability, amphipathicity, hydrophobicity, and serum stability are key factors as well as their ability to cross the membrane and reach intracellular targets. Shorter peptides may not only imply a reduction in cost production but may also be considered as more efficient in crossing the plasmatic membrane and exerting a cytotoxic effect [5,11]. For instance, FK16, a peptide derived from LL-37, a helical peptide known to possess anticancer effects on gastric cancer and T leukemic cells, showed higher anticancer activity than the full-length peptide itself [32]. Therefore, identifying the amino acids responsible for the anticancer activity may facilitate the synthesis, increase efficiency and impact in the cost production by allowing the synthesis of shorter peptides that retain full biological activity. CIGB-552 is a novel peptide whose 20 amino acid sequence is the result of modifications of AMP derived peptide, L2 [8]. Being characterized through several approaches, its cell penetrating capacity plays a major role in its mode of action because one of the main characterized targets so far is the COMMD1 protein, ubiquitously located in the cytoplasm [2,8]. Subcutaneous administration of CIGB-552 in tumor-bearing mice not only results in a reduction of tumor volume and increased lifespan, without side effects as indicated by body weight, but also in accumulation of the peptide in tumors. Furthermore, a serine-protease degradation pattern for the peptide in BALB/c mice serum was identified [7,9]. CIGB-552 derived metabolites, although preliminary characterized regarding their cytotoxicity and cell-penetrating capability, were not subjected to proper characterization in order to determine their similarities and differences to CIGB-552. First, cell-penetrating

Table 4. Summary of the properties evaluated for CIGB-552 and its derived metabolites.

ID	Sequence	Pro-apoptotic effect	COMMD1-binding interaction	Cell penetrating capacity	Lipid binding capacity	Secondary structure (β-sheet/α-helix)
CIGB-552	HARIKPTFRRLKWKYKGKFW	+++	+++	+++	+	–
5	IKPTFRRLKWKYKGKFW	–	++	++	+	–
1a	IKPTFRRLKWKYKG	–	–	+	–	–
3	IKPTFRRLKW	–	–	+	–	–

probability, physicochemical properties, and structure predictions were analyzed using a theoretical approach. Our first results showed that despite the fact that sequence differences are found among CIGB-552 and its derived metabolites all retain the same probability to be considered as cell-penetrating peptides. Only the net charge was markedly reduced in the metabolites, and this property plays an important role when peptide–lipid interactions are based on electrostatic interactions [1,3–5,20,21]. Despite charge reduction no other significant differences were found among CIGB-552 and the metabolites. However, when tested for their cytotoxic capacities, we found that the derived metabolites presented higher IC_{50} values than CIGB-552. Furthermore, under conditions in which CIGB-552 (300 μM) confirmed its pro-apoptotic properties, metabolites failed to elicit apoptosis in the MCF-7 cell line. In addition, we found that neither the interaction with COMMD1 nor the cell penetrating capabilities are as effective in the derived metabolites as in the CIGB-552 peptide itself. Therefore, these findings could explain why metabolites failed to elicit apoptosis in the MCF-7 cell line. As it was mentioned before, CPPs such as CIGB-552 may use two different internalization mechanisms, transduction and endocytosis, which can be either identified by the internalization pattern or by the conditions required to occur [25,26]. Here, we show for the first time that both mechanisms appear to be present in CIGB-552 and its derived metabolites as observed both by confocal microscopy and flow cytometry assays performed at different temperatures. However, each internalization mechanism seems to have a different impact among CIGB-552 and its derived metabolites. Results obtained from both the frequency of the *transduction-like* pattern (fully loaded cells) and temperature effect indicate that even though CIGB-552 actually uses endocytosis, a major contribution of transduction is observed. On the other hand, the effect of transduction in derived metabolites is lower than in CIGB-552 indicating that endocytosis may be the preferred mechanism. Transduction has been described as an energy-independent process where peptides concentrate in the outer leaflet and upon reaching certain concentration levels a transient and very fast internalization occurs through different mechanism [33,34]. Peptide structure and lipid affinity play key roles in the transduction capability. Therefore, by performing isothermal titration calorimetry, we were able to identify binding-like patterns for CIGB-552 and metabolite 5. Although, mechanisms as well as affinities involved may vary among them, the results shown here are not sufficient to prove so; more assays will be required. Given the amino acid sequences for the metabolites and the CIGB-552, we can point out three different amino acids which have been reported as important players, forming small consensus sequences, in membrane interaction and cell-penetrating capacity of CPPs: lysine, arginine, and tryptophan [35–37]. Although lysine containing peptides are efficiently internalized, membrane insertion has been proven to be greater when polyarginine sequences are present in the peptide [36,38]. On the other hand, it has been reported that the presence of tryptophan in the peptides backbones confers higher cell-penetrating capacity when they are distributed along the sequence [37]. Regarding structural conformation, data reported for different CCPs indicates that they may adopt several conformations: α-helical, β-sheet, looped, or even extended [21]. Molecular dynamics simulations performed here suggest that none of the peptides studied show a marked tendency to stably adopt secondary structure elements, neither in aqueous nor in membrane environment (summary of the properties evaluated is shown in Table 4). However, we observed that the presence of aromatic residues only present at the C-termini of CIGB-552 and metabolite 5 translates in the formation of a hydrophobic cluster that ultimately results in a looped structure stabilized by the formation of a stiff salt bridge between an arginine and the COO^- moiety. Although the maximum affordable time scale of the simulations differs significantly from experimental times, this structural organization could help internalization by reducing the free energy needed to translocate the C-terminal carboxylate [31]. Moreover, the looped conformation conserved in the two longest peptides offers a putative explanation for the similar characteristics displayed in contrast with metabolites 1 and 3a in terms of enhanced membrane interaction, internalization, and cytotoxic activity. In conclusion, peptide CIGB-552 and metabolite 5 have similar behavior regarding the characteristics evaluated. However because of its higher affinity for COMMD1, CIGB-552 still shows the highest effectiveness emerging as the minimum active sequence needed to produce marked effects in a human tumor-derived cell line such as the MCF-7 cell line.

Conflict of Interests

The authors declare that there is no conflict of interests regarding the publication of this paper.

Acknowledgements

This project was funded by FOCEM (MERCOSUR Structural Convergence Fund), COF 03/11. SA would like to acknowledge PhD. Leonel Malacrida for kindly providing lipid reagents and support in liposome synthesis. Thanks to Prof. Ana Denicola from Facultad de Ciencias (UdelaR) for the use of the Chronos FD spectrofluorometer (ISS, Champaign, IL). Financial support was provided by ANII (PhD fellowship POS_NAC_2012_1_8523).

References

1 Zasloff M. Antimicrobial peptides of multcellular organisms. *Nature* 2002; **415**: 389–395.

2 Burstein E, Hoberg JE, Wilkinson AS, Rumble JM, Csomos RA, Komarck CM, Maine GN, Wilkinson JC, Mayo MW, Duckett CS. COMMD proteins, a novel family of structural and functional homologs of MURR1. *J. Biol. Chem.* 2005; **280**: 22222–22232. DOI: 10.1074/jbc.M501928200.

3 Hoskin DW, Ramamoorthy A. Studies on anticancer activities of antimicrobial peptides. *Biochim. Biophys. Acta* 2008; **1778**: 357–375. DOI: 10.1016/j.bbamem.2007.11.008.
4 Li Y, Xiang Q, Zhang Q, Huang Y, Su Z. Overview on the recent study of antimicrobial peptides: origins, functions, relative mechanisms and application. *Peptides* 2012; **37**: 207–215. DOI: 10.1016/j.peptides.2012.07.001.
5 Gaspar D, Salomé Veiga A, Castanho MARB. From antimicrobial to anticancer peptides. A review. *Front. Microbiol.* 2013; **4**: 1–16. DOI: 10.3389/fmicb.2013.00294.
6 Blanco-Míguez A, Gutiérrez-Jácome A, Pérez-Pérez M, Pérez-Rodríguez G, Catalán-García S, Fdez-Riverola F, Lourenço A, Sánchez B. From amino acid sequence to bioactivity: scientific evidence on antitumor peptides. *Protein Sci.* 2016; **25**: 1084–1095. DOI: 10.1002/pro.2927.
7 Vallespi MG, Fernandez JR, Torrens I, Garcia I, Garay H, Mendoza O, Granadillo M, Falcon V, Acevedo B, Ubieta R, Guillen GE, Reyes O. Identification of a novel antitumor peptide based on the screening of an Ala-Library derived from the LALF(32-51) region. *J. Pept. Sci.* 2010; **16**: 40–47. DOI: 10.1002/psc.1192.
8 Fernández Massó JR, Oliva Argüelles B, Tejeda Y, Astrada S, Garay H, Reyes O, Delgado-Roche L, Bollati-Fogolín M, Vallespí MG. The antitumor peptide CIGB-552 increases COMMD1 and inhibits growth of human lung cancer cells. *J. Amino Acids* 2013; **2013**: 251398. DOI: 10.1155/2013/251398.
9 Vallespí MG, Pimentel G, Cabrales-Rico A, Garza J, Oliva B, Mendoza O, Gomez Y, Basaco T, Sánchez I, Calderón C, Rodriguez JC, Markelova MR, Fichtner I, Astrada S, Bollati-Fogolín M, Garay HE, Reyes O. Antitumor efficacy, pharmacokinetic and biodistribution studies of the anticancer peptide CIGB-552 in mouse models. *J. Pept. Sci.* 2014; **20**: 850–859. DOI: 10.1002/psc.2676.
10 de Bie P, van de Sluis B, Burstein E, Duran KJ, Berger R, Duckett CS, Wijmenga C, Klomp LWJ. Characterization of COMMD protein–protein interactions in NF-kappaB signalling. *Biochem. J.* 2006; **398**: 63–71. DOI: 10.1042/BJ20051664.
11 Vlieghe P, Lisowski V, Martinez J, Khrestchatisky M. Synthetic therapeutic peptides: science and market. *Drug Discov. Today* 2010; **15**: 40–56. DOI: 10.1016/j.drudis.2009.10.009.
12 Vichai V, Kirtikara K. Sulforhodamine B colorimetric assay for cytotoxicity screening. *Nat. Protoc.* 2006; **1**: 1112–1116. DOI: 10.1038/nprot.2006.179.
13 Skehan P, Storeng R, Scudiero D, Monks A, Vistica D, Warren JT, Bokesch H, Boyd MR. New colorimetric cytotoxicity assay for anticancer-drug screening. *J. Natl. Cancer Inst.* 1990; **82**: 1107–1112.
14 de Chaumont F, Dallongeville S, Chenouard N, Hervé N, Pop S, Provoost T, Meas-Yedid V, Pankajakshan P, Lecomte T, Le Montagner Y, Lagache T, Dufour A, Olivo-Marin J-C. Icy: an open bioimage informatics platform for extended reproducible research. *Nat. Methods* 2012; **9**: 690–696. DOI: 10.1038/nmeth.2075.
15 Darré L, Machado MR, Brandner AF, González HC, Ferreira S, Pantano S. SIRAH: a structurally unbiased coarse-grained force field for proteins with aqueous solvation and long-range electrostatics. *J. Chem. Theory Comput.* 2015; **11**: 723–739. DOI: 10.1021/ct5007746.
16 Machado MR, Pantano S. SIRAH tools: mapping, backmapping and visualization of coarse-grained models. *Bioinformatics* 2016; **32**: 1568–1570. DOI: 10.1093/bioinformatics/btw020.
17 Yin H, Moulton H, Betts C, Wood M. CPP-directed oligonucleotide exon skipping in animal models of duchenne muscular dystrophy. *Methods Mol Biol* 2011; **683**: 321–338. DOI:10.1007/978-1-60761-919-2_23.
18 Tang H, Su Z-D, Wei H-H, Chen W, Lin H. Prediction of cell-penetrating peptides with feature selection techniques. *Biochem. Biophys. Res. Commun.* 2016; **477**: 150–154. DOI: 10.1016/j.bbrc.2016.06.035.
19 Singh S, Singh H, Tuknait A, Chaudhary K, Singh B, Kumaran S, Raghava GPS. PEPstrMOD: structure prediction of peptides containing natural, non-natural and modified residues. *Biol. Direct* 2015; **10**: 73. DOI: 10.1186/s13062-015-0103-4.
20 Madani F, Lindberg S, Langel Ü, Futaki S, Gräslund A. Mechanisms of cellular uptake of cell-penetrating peptides. *J. Biophys.* 2011; **2011**: 414729. DOI: 10.1155/2011/414729.
21 Milletti F. Cell-penetrating peptides: classes, origin, and current landscape. *Drug Discov. Today* 2012; **17**: 850–860. DOI: 10.1016/j.drudis.2012.03.002.
22 Wlodkowic D, Telford W, Skommer J, Darzynkiewicz Z. *Apoptosis and Beyond: Cytometry in Studies of Programmed Cell Death*, Vol. **103**. Elsevier Inc.: San Diego, USA 2011; DOI:10.1016/B978-0-12-385493-3.00004-8.
23 Liang Y, Yan C, Schor NF. Apoptosis in the absence of caspase 3. *Oncogene* 2001; **20**: 6570–6578. DOI: 10.1038/sj.onc.1204815.
24 Mc Gee MM, Hyland E, Campiani G, Ramunno A, Nacci V, Zisterer DM. Caspase-3 is not essential for DNA fragmentation in MCF-7 cells during apoptosis induced by the pyrrolo-1,5-benzoxazepine, PBOX-6. *FEBS Lett.* 2002; **515**: 66–70. DOI: 10.1016/S0014-5793(02)02440-7.
25 Ter-Avetisyan G, Tünnemann G, Nowak D, Nitschke M, Hermann A, Drab M, Cardoso MC. Cell entry of arginine-rich peptides is independent of endocytosis. *J. Biol. Chem.* 2009; **284**: 3370–3378. DOI: 10.1074/jbc.M805550200.
26 Tünnemann G, Ter-avetisyan G, Martin RM, Stockl M, Herrmann A, Cardoso MC. Live-cell analysis of cell penetration ability and toxicity of oligo-arginines. *J. Pept. Sci.* 2008; **14**: 469–476. DOI: 10.1002/psc.
27 Bucci C, Parton RG, Mather IH, Stunnenberg H, Simons K, Hoflack B, Zerial M. The small GTPase rab5 function as a regulatory factor in the early endocytic pathway. *Cell* 1992; **70**: 715–728.
28 Rodriguez-Corona U, Sobol M, Rodriguez-Zapata LC, Hozak P, Castano E. Fibrillarin from archaea to human. *Biol. Cell* 2015; **107**: 1–34. DOI: 10.1111/boc.201400077.
29 Leavitt S, Freire E. Direct measurement of protein binding energetics by isothermal titration calorimetry. *Curr. Opin. Struct. Biol.* 2001; **11**: 560–566. DOI: 10.1016/S0959-440X(00)00248-7.
30 Herce HD, Garcia AE. Molecular dynamics simulations suggest a mechanism for translocation of the HIV-1 TAT peptide across lipid membranes. *Proc. Natl. Acad. Sci. U. S. A.* 2007; **104**: 20805–20810. DOI: 10.1073/pnas.0706574105.
31 Lazaridis T, Leveritt J, III, PeBenito L. Implicit membrane treatment of buried charges groups: application to peptide translocation across lipid bilayers. *Biochim. Biophys. Acta* 2014; **1838**: 2149–2159. DOI: 10.1002/bit.25180.Synthetic.
32 Ren SX, Shen J, Cheng ASL, Lu L, Chan RLY, Li ZJ, Wang XJ, Wong CCM, Zhang L, Ng SSM, Chan FL, Chan FKL, Yu J, Sung JJY, Wu WKK, Cho CH. FK-16 derived from the anticancer peptide LL-37 induces caspase-independent apoptosis and autophagic cell death in colon cancer cells. *PloS ONE* 2013; **8**: 1–9; DOI:10.1371/journal.pone.0063641.
33 Melo MN, Ferre R, Castanho MA. Antimicrobial peptides: linking partition, activity and high membrane-bound concentrations. *Nat. Rev. Microbiol.* 2009; **7**: 245–250. DOI: 10.1038/nrmicro2095.
34 Bechara C, Sagan S. Cell-penetrating peptides: 20 years later, where do we stand? *FEBS Lett.* 2013; **587**: 1693–1702. DOI: 10.1016/j.febslet.2013.04.031.
35 Futaki S, Suzuki T, Ohashi W, Yagami T, Tanaka S, Ueda K, Sugiura Y. Arginine-rich peptides. An abundant source of membrane-permeable peptides having potential as carriers for intracellular protein delivery. *J. Biol. Chem.* 2001; **276**: 5836–5840. DOI: 10.1074/jbc.M007540200.
36 Takechi Y, Yoshii H, Tanaka M, Kawakami T, Aimoto S, Saito H. Physicochemical mechanism for the enhanced ability of lipid membrane penetration of polyarginine. *Langmuir* 2011; **27**: 7099–7107. DOI: 10.1021/la200917y.
37 Rydberg HA, Matson M, Åmand HL, Esbjörner EK, Norde B. Effect of tryptophan content and backbone spacing on the uptake efficiency of cell-penetrating peptides. *Biochemistry* 2012; **51**: 5531–5539.
38 Mitchell DJ, Kim DT, Steinman L, Fathman CG, Rothbard JB. Polyarginine enters cells more efficiently than other polycationic homopolymers. *J. Pept. Res.* 2000; **56**: 318–325. DOI: 10.1034/j.1399-3011.2000.00723.x.

Supporting information

Additional supporting information may be found in the online version of this article at the publisher's web site.

Table 1. CPP capacity prediction
Table 2. Cytotoxicity of CIGB-552 evaluated by SRB assay in different tumor cell lines [1].
Table 3. Area per lipid, thickness, and lateral diffusion coefficient measured at 27 °C over 1 μs of trajectory. Experimental values and atomistic simulation from the literature are remarked in the second and third rows, respectively.
Figure S1. A, B Caspase and Annexin V staining, respectively. FSC *versus* SSC, Caspase-FITC *versus* FSC or Annexin V-FITC *versus* SSC

representative dot plots are shown. Positive-stained population is shown in green. C, Fold change between CIGB-552 treated cells to the control observed for both Caspase 7 and Annexin V positive cells.
Figure S2. Anti-proliferative dose–response curves for CIGB-552 and its analogous metabolites in MCF-7 cancer cell line. SRB assay was performed in order to determine cytotoxic capacity of metabolites compared to CIGB-552. IC50 values obtained are provided in the manuscript (Table 2).
Figure S3. FITC fluorescence intensity histograms obtained from the internalization of different concentrations of CIGB-552-FITC after 1 h of incubation at 37 °C in the MCF-7 cell line. Changes observed in the profile of the histograms revealed the appearance of two intensity peaks for concentrations higher than 50 μM.
Figure S4. A, Center of mass analysis for CIGB-552 and its derived metabolites from 0.5 to 128 μM. B, Center of mass analysis for CIGB-552 at higher concentrations (31.25 to 1000 μM).
Figure S5. Co-localization between Rab5A and CIGB-552 derived metabolites. A, metabolite 5. B, metabolite 1a. C, metabolite 3. Arrow heads indicate co-localization (scale bar = 10 μm).
Figure S6. Atomistic and CG representations of DMPC. The non-bonded interaction's parameters are indicated for each bead. Charges are indicated in electron units while vdW parameters are in nm and kJ/mol for sigma and epsilon, respectively. The asterisk on the choline bead indicates that, as the side chain of Lys, it also establishes vdW interactions not calculated according to the Lorentz–Berthelot combination rules [2].
Figure S7. A, Density profile distributions of both DMPC and water. B, Density profile distribution of both phosphate head group, K^+ and Cl^-. Values were measured at 27 °C over the last 500 ns of trajectory. Representative snapshot of the MD simulation. C, DMPC acyl chains, phosphates, and choline beads are represented in white, red, and blue lines, respectively. K^+ ions are colored in blue, while Cl^- ions are depicted in green. Water is drawn with turquoise dots.